ACS APPLIED MATERIALS & INTERFACES

Research Article

www.acsami.org

Photochromism-Induced Amplification of Critical Current Density in Superconducting Boron-Doped Diamond with an Azobenzene Molecular Layer

Keisuke Natsui,[†] Takashi Yamamoto,*[,†] Miku Akahori,[†] and Yasuaki Einaga*[,†,‡]

[†]Department of Chemistry, Keio University, 3-14-1 Hiyoshi, Yokohama 223-8522, Japan

[‡]JST-CREST, 3-14-1 Hiyoshi, Yokohama 223-8522, Japan

ABSTRACT: A key issue in molecular electronics is the control of electronic states by optical stimuli, which enables fast and high-density data storage and temporal-spatial control over molecular processes. In this article, we report preparation of a photoswitchable superconductor using a heavily boron-doped diamond (BDD) with a photochromic azobenzene (AZ) molecular layer. BDDs electrode properties allow for electrochemical immobilization, followed by copper(I)-catalyzed alkyne−azide cycloaddition (a "click" reaction). Superconducting properties were examined with magnetic and electrical transport measurements, such as field-dependent isothermal magnetization, temperature-dependent resistance, and the low-temperature voltage−current response. These measurements revealed reversible amplification of the critical current density by 55% upon photoisomerization. This effect is explained as the reversible photoisomerization of AZ inducing an inhomogeneous electron distribution along the BDD surface that renormalizes the surface pinning contribution to the critical current.

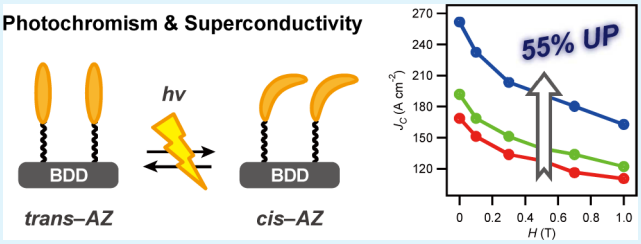

KEYWORDS: *photoswitching, critical current density, azobenzene, boron-doped diamond, electrochemistry, click chemistry*

INTRODUCTION

Photoswitchable systems are important in various fields, such as molecular science,[1−3] materials chemistry,[4−6] and biotechnology,[7−9] because the use of light enables fast, high-density data storage[10,11] and temporal−spatial control over molecular processes.[12,13] Photochromism is the reversible phototransformation of a chemical species between isomers that have different absorption spectra.[14] As a result of the photochromic reaction (photoisomerization), physicochemical properties may also change, including dielectric constant, electrochemical potentials, and geometrical structures. Therefore, photochromic molecules have been widely used as building blocks for fabricating photoswitchable materials, and some notable examples are conductance photoswitching in the diarylethene−gold nanoparticle network,[15,16] "remote-control" photoswitching of dithienylethene in the presence of photon upconverting nanoparticles,[17,18] and photoswitchable field-effect transistors using azobenzene[19] and spiropyran.[20] Our research group has focused on developing photoswitchable magnetic materials that use azobenzene as a molecular switch, and reversible photoswitching of magnetization is present in nanoparticles[21,22] and nanofilms.[23−26] Generically, photoswitchable materials can be fabricated by the appropriate integration of photochromic compounds and functional materials.

Since the discovery of vanishing resistance in mercury,[27] superconducting materials have attracted considerable attention for both fundamental aspects[28,29] and potential applications.[30,31] Most superconductivity research either investigates new classes of materials,[32] improves existing properties,[33] or probes the nature of the many-body state.[34] Molecular electronics often looks to control electronic states by external stimuli. For superconductors, the field-effect transistor structure has been applied to modulate the surface carrier density.[35−37] In addition, charge transfer at the interface of organic−inorganic hybrids can induce a field-effect-like behavior,[38] modulating conducting properties of metals,[39] semiconductors,[40] and even superconductors.[41] Recently, on the basis of the above principle, we modulated the superconducting critical current in an azobenzene-immobilized niobium thin film.[42] Azobenzene undergoes a reversible *cis*−*trans* isomerization upon photoirradiation, where the molecular dipole moments are different for *trans*- and *cis*-isomers.[43] In azobenzene-immobilized niobium thin films, these dipole moment changes modify the niobium work function to modulate the critical current. In other words, the reversible photoisomerization of immobilized azobenzene induces charge transfer at the niobium interface. More recently, the superconducting critical temperature (T_C) was modulated in an yttrium barium copper oxide film by immobilized photoresponsive materials.[44]

In 2004, a heavily boron-doped diamond (BDD) was found to be a superconductor with a T_C of 2.3 K.[45] Inspired by McMillan's equation, $T_C \approx \theta \exp[-(1 + \lambda)/\lambda]$, where λ is an

Received: October 27, 2014
Accepted: December 10, 2014
Published: December 10, 2014

Scheme 1. Synthesis of 4-((Triisopropylsilyl)ethynyl)aniline

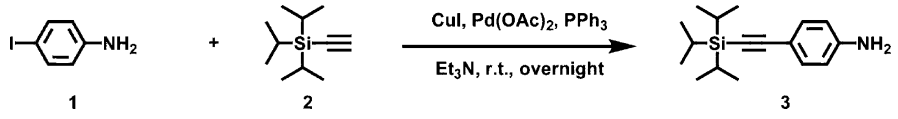

electron−phonon interaction constant, and θ is the Debye temperature,[46] the high Debye temperature diamond is considered a candidate of high-temperature superconductivity. Therefore, superconducting diamonds have attracted a lot of attention, mainly for fundamental superconducting properties and theory.[47] In 2009, a single crystalline BDD film with (111) orientation exhibited a T_C > 10 K and an upper critical field ($H_{C,2}$) > 15 T.[47] The T_C of BDD can also be enhanced by increasing boron (carrier) concentration. Furthermore, the diamond surface can be modified by chemical treatments, such as UV ozone irradiation, electrochemical redox reactions, exposure to halogen gases, and others.[48] These treatments can affect the diamond properties, for example, changing between a hydrogen- and oxygen-terminated diamond drastically varies the surface conductivity.[49] Exploiting this mode of thinking, we recently reported the reversible modulation of the superconducting critical current density of BDD by changing surface termination between hydrogen and oxygen.[50] As we have shown that superconductivity in BDD is sensitive to its surface state, even in a 10 μm thick film, photoswitching of superconducting BDD by surface modification with a photochromic molecule is an attractive proposition.

Herein, we report preparation and superconducting properties of a boron-doped diamond immobilized with a photochromic azobenzene molecular layer. Since BDD is a stable, conductive electrode, we employed electrochemical immobilization,[51] followed by copper(I)-catalyzed alkyne−azide cycloaddition (a "click" reaction).[52] Immobilization of azobenzene was monitored by cyclic voltammetry (CV) and X-ray photoelectron spectroscopy (XPS). Photoisomerization of immobilized azobenzene molecules were monitored by CV using $K_4[Fe^{II}(CN)_6]/K_3[Fe^{III}(CN)_6]$ redox couples as probes for electron transfer at the BDD surface. Superconducting properties were examined with magnetic and electrical transport measurements, such as field-dependent isothermal magnetization, temperature-dependent resistance, and the low-temperature voltage−current response. As a result, we observed a 55%, reversible amplification of the critical current density upon photoisomerization.

EXPERIMENTAL SECTION

Materials. All reagents are commercially available and used without any further purification.

4-((Triisopropylsilyl)ethynyl)aniline (Compound 3). Compound **3** was synthesized as described in the literature (Scheme 1).[53] 4-Iodoaniline (**1**; 4.99 g, 22.8 mmol) was dissolved in triethylamine (50 mL), and the solution was degassed by boiling briefly under reduced pressure, followed by flushing with argon. Under argon atmosphere, copper(I) iodide (0.0461 g, 0.242 mmol), palladium(II) acetate (0.103 g, 0.459 mmol), and triphenylphosphine (0.260 g, 0.991 mmol) were added to the above solution, followed by the addition of trimethylsilylacetylene (**2**; 4.02 g, 4.95 mL, 22.1 mmol). After stirring at room temperature overnight, hexane was added, and triethylaminehydrogen iodide was removed by filtration through Celite. The filtrate was evaporated and then purified by chromatography on silica, eluting with 10:1 hexane/ethyl acetate, which gave a brown oil of **3** (6.03 g, 83%). ^{1}H NMR (400 MHz, $CDCl_3$, TMS): δ (ppm) = 7.28 (2H, d, J = 8.9 Hz), 6.57 (2H, d, J = 9.0 Hz), 3.78 (2H, s), 1.11 (21H, s).

4-((Triisopropylsilyl)ethynyl)benzenediazonium Tetrafluoroborate (Compound 4). Compound **4** was synthesized as described in the literature (Scheme 2).[51] Compound **3** (1.37 g, 5.01 mmol) was

Scheme 2. Synthesis of 4-((Triisopropylsilyl)ethynyl)benzenediazonium Tetrafluoroborate

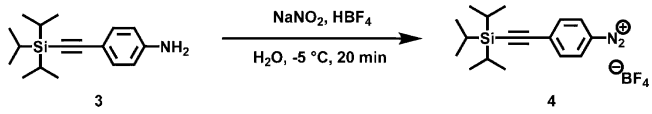

dissolved in aqueous tetrafluoroboric acid (9 mL, 25 wt %). After this solution was cooled at −5 °C, a cooled solution of sodium nitrite (0.520 g, 7.52 mmol) in distilled water (1 mL) was slowly added while vigorously stirring. The solution was stirred at −5 °C for 20 min and then at room temperature for 20 min. The precipitate was filtered and washed with a 5% aqueous solution of sodium tetrafluoroborate, cold water, cold methanol, and diethyl ether, which gave a beige solid of **4** (1.87 g, 79%). ^{1}H NMR (400 MHz, $CDCl_3$, TMS): δ (ppm) = 8.57 (2H, d, J = 9.2 Hz), 7.79 (2H, d, J = 9.4 Hz), 1.11 (s, 21H).

4,4′-Dihydroxyazobenzene (Compound 6). Compound **6** was synthesized as described in literature (Scheme 3).[54] A mixture of

Scheme 3. Synthesis of 4,4′-Dihydroxyazobenzene

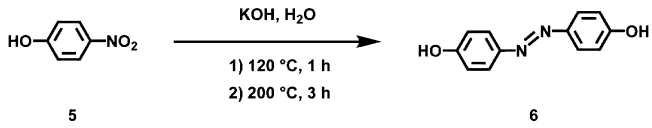

p-nitrophenol (**5**; 10.0 g, 71.9 mmol), potassium hydroxide (49.7 g, 886 mmol), and water (10 mL) was heated to 120 °C for 1 h and at 200 °C for 3 h. After the solution cooled, remaining solids were dissolved in water, followed by acidification to pH ≈ 1 with concentrated hydrochloric acid. The mixture was extracted with diethyl ether (washed with water and brine) and dried over sodium sulfate. The solvent was evaporated, and the residue was recrystallized from 1:1 ethanol/water to give a yellow brown powder of **6** (3.99 g, 52%). ^{1}H NMR (400 MHz, CD_3OD, TMS): δ (ppm) = 7.74 (4H, d, J = 12 Hz), 6.88 (4H, d, J = 8.0 Hz), 4.86 (s, 1H).

4-((4-(2-Chloroethoxy)phenyl)diazenyl)phenol (Compound 8). Sodium hydride (0.203 g, 60% dispersion, 5.07 mmol) was suspended in absolute dimethylformamide (32 mL) after washing with hexane under argon atmosphere. Compound **6** (1.07 g, 5.01 mmol) was added to the mixture at room temperature and stirred for 2 h. 1,2-Dichloroethane (**7**; 8.77 g, 7 mL, 88.6 mmol) was then added (see Scheme 4), and the mixture was vigorously stirred at 60 °C for 47 h. After it cooled, the mixture was extracted with diethyl ether (washed with water and brine) and dried over sodium sulfate. The solvent was evaporated, and then the mixture was purified by chromatography on silica, eluting with 3:1 hexane/ethyl acetate, which gave an orange powder of **8** (0.192 g, 14%). ^{1}H NMR (400 MHz, $CDCl_3$, TMS): δ (ppm) = 7.87 (2H, d, J = 9.2 Hz), 7.84 (2H, d, J = 9.0 Hz), 7.02 (2H, d, J = 9.0 Hz), 6.93 (2H, d, J = 9.0 Hz), 4.31 (2H, t, J = 5.8 Hz), 3.85 (2H, t, J = 5.8 Hz).

4-((4-(2-Azidoethoxy)phenyl)diazenyl)phenol (Compound 9). Compound **8** (0.192 g, 0.695 mmol) and sodium azide (0.110 g, 1.70 mmol) were dissolved in dimethylformamide (22 mL) and stirred at 100 °C for 3.5 h (see Scheme 5). After it cooled, the mixture was extracted with diethyl ether (washed with a saturated sodium

dx.doi.org/10.1021/am5074613 | ACS Appl. Mater. Interfaces 2015, 7, 887−894

Scheme 4. Synthesis of 4-((4-(2-Chloroethoxy)phenyl)diazenyl)phenol

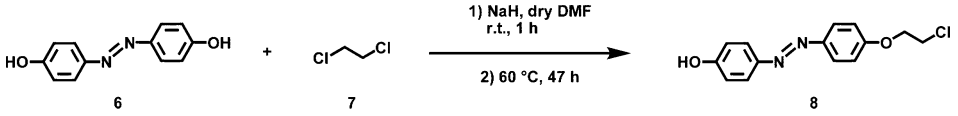

Scheme 5. Synthesis of 4-((4-(2-Azidoethoxy)phenyl)diazenyl)phenol

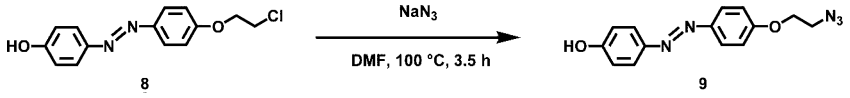

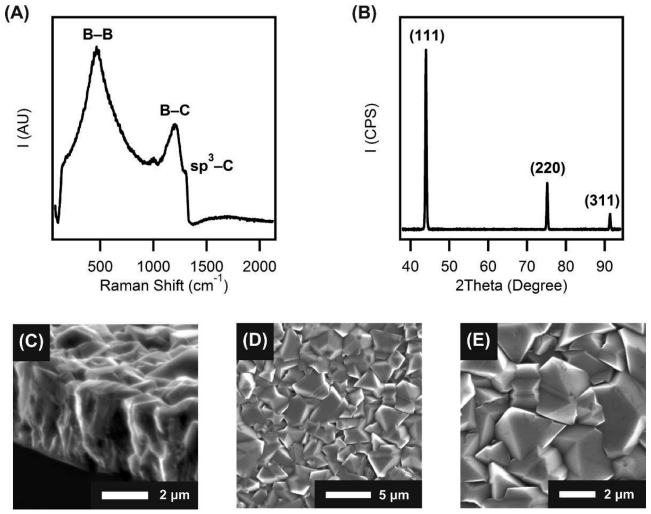

Figure 1. Structure of an as-deposited BDD. (A) The Raman spectrum showed two dominant bands due to heavy doping of boron. (B) XRD patterns confirmed the diamond cubic structure. (C) A cross-sectional SEM image. (D, E) Surface SEM images show the BDD morphology.

bicarbonate aqueous solution, water, and brine) and dried over sodium sulfate. Evaporation of the solvent gave a yellow powder of **9** (0.176 g, 89%). ^{1}H NMR (400 MHz, $CDCl_3$, TMS): δ (ppm) = 7.88 (2H, d, J = 8.0 Hz), 7.84 (2H, d, J = 8.0 Hz), 7.03 (2H, d, J = 12 Hz), 6.94 (2H, d, J = 12 Hz), 4.23 (2H, t, J = 4.0 Hz), 3.65 (2H, t, J = 6.0 Hz).

Boron-Doped Diamond. BDD was synthesized as described in the previous report.[50] BDD was deposited onto a silicon wafer substrate by a microwave plasma-assisted chemical vapor deposition method with a commercial microwave plasma reactor (5 kW, ASTeX Inc.). Deposition was carried out for 8 h under 100 Torr of chamber pressure, 4500 W microwave power, and 900−1000 °C substrate temperature.

Methods. ^{1}H NMR spectra were obtained using JNM-AL400 (JEOL). Structure of BDD was characterized by Raman spectroscopy (excitation wavelength: 532 nm) and X-ray diffraction (XRD). The XRD patterns were recorded on a D8 Discover (Bruker) using a Ni-filtered Cu Kα line radiation, and the Raman spectrum was recorded with Acton SP2500 (Princeton Instruments). Surface morphology was examined with a field emission scanning electron microscope (FE-SEM) using SIRION (FEI). Electrochemical measurements were carried out in a single compartment cell at room temperature, using a conventional three-electrode system: BDD as a working electrode, a platinum wire as a counter electrode, and Ag/AgCl (saturated KCl) as a reference electrode. Cyclic voltammetry (CV) was recorded by a CompactStat potentiostat (Ivium Technologies). Surface modification processes were confirmed by X-ray photoelectron spectroscopy (XPS) using JPS-9000MC (JEOL) equipped with a Mg Kα line source. Superconducting properties were investigated with magnetic measurements and electrical transport measurements using a four-terminal method by a superconducting quantum interference device (SQUID) magnetometer (MPMS-XL, Quantum Design) and SourceMeter 2400

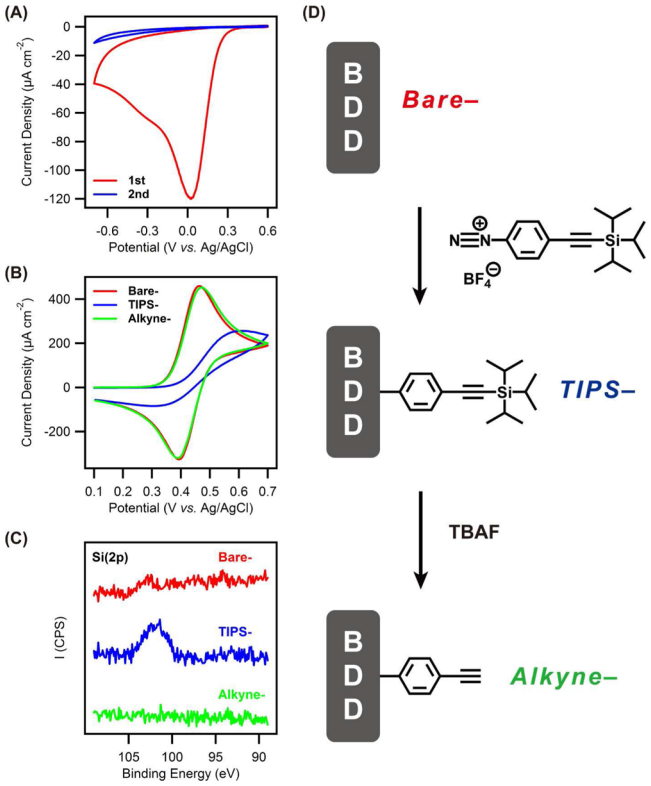

Figure 2. Preparation of alkyne-terminated BDD. (A) CVs in an acetonitrile solution of the diazonium salt confirmed complete immobilization after second cycle (blue). (B) CVs in an acetonitrile solution of ferrocene: (red) bare-, (blue), TIPS-, and (green) alkyne-terminated BDD, respectively. The immobilized organic layer is thin and presents a low barrier for electron transfer. (C) XPS spectra showed the Si(2p) peak was clearly observed in TIPS-terminated BDD (blue) and disappeared in alkyne-terminated BDD (green). (D) A schematic illustration of preparing alkyne-terminated BDD.

and NanovoltMeter 2182A (Keithley) in a SQUID magnetometer, respectively. UV light irradiation (filtered light, λ_{max} = 360 nm, 6.5 mW cm^{-2}) was carried out using an ultrahigh-pressure mercury lamp (Spot Cure SP-7, USHIO), and visible light irradiation (λ = 400−700 nm, 45 mW cm^{-2}) was carried out using a xenon lamp (Optical Modulex X 500, USHIO).

RESULTS AND DISCUSSION

First, we characterized BDD on silicon by using Raman, XRD, and SEM. The Raman spectrum (Figure 1A) showed two dominant bands at ∼500 and 1200 cm^{-1}, typically observed in BDD, which are assigned to B−B and B−C vibrations, respectively.[55] XRD patterns (Figure 1B) showed three sharp peaks at 2θ = 44.0°, 75.2°, 91.4°, corresponding to (111), (220), and (311) diffractions, respectively, which confirmed the diamond

dx.doi.org/10.1021/am5074613 | ACS Appl. Mater. Interfaces 2015, 7, 887−894

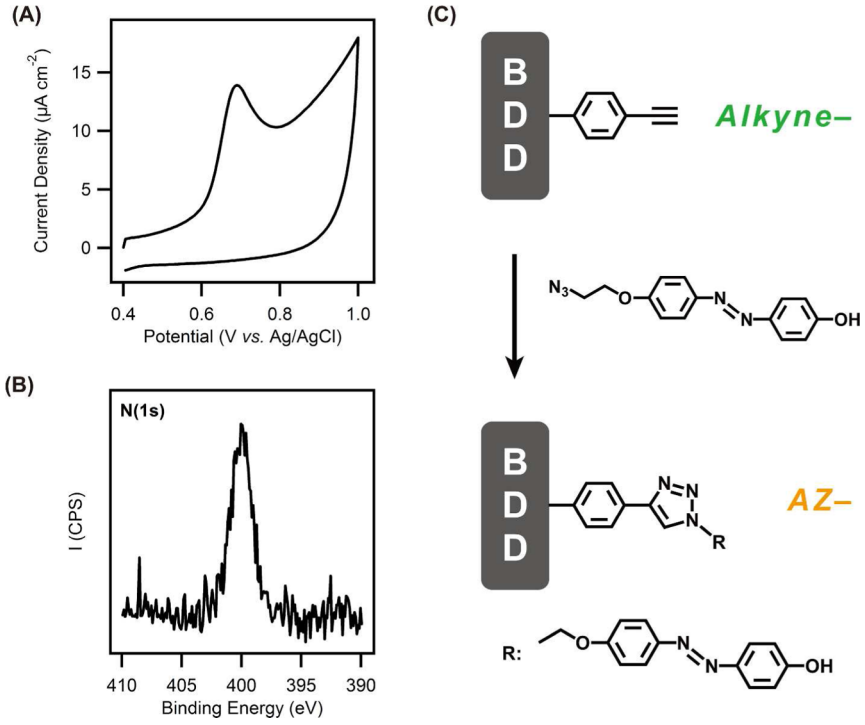

Figure 3. Immobilization of AZ onto alkyne-terminated BDD. (A) CV of AZ-terminated BDD showed oxidation of a phenolic hydroxyl group of AZ. (B) The XPS spectrum showed a strong N(1s) peak from a triazole ring and AZ. (C) A schematic illustration of preparing AZ-terminated BDD.

cubic structure with a lattice constant of 3.57 Å. From SEM images, BDD was estimated to be ca. 4 μm thick (Figure 1C) and showed a polycrystalline nature with a grain size of ca. 2 μm (Figure 1D,E).

Azobenzene (AZ) was immobilized onto a BDD surface by three steps. As the first step, the diazonium salt (4-((triisopropylsilyl) ethynyl)benzenediazonium tetrafluoroborate) was covalently immobilized by an electroreduction reaction. The electroreduction was performed using CV in an acetonitrile solution of the diazonium salt (10 mM) and tetrabutylammonium hexafluorophosphate (0.1 M) with a scan rate of 50 mV s^{-1} between +0.60 and −0.75 V (vs Ag/AgCl). A clear reduction peak was observed at +0.06 V (Figure 2A), and the peak current disappeared after the second cycle, indicating inhibition of electron transfer between BDD and a bulky diazonium salt. As the second step, alkyne-terminated BDD was prepared by deprotection of the triisopropylsilyl (TIPS) group at a BDD surface. Deprotection was performed by immersing TIPS-terminated BDD in a tetrahydrofuran solution of tetrabutylammonium fluoride (50 mM) for 20 min at room temperature. These processes were monitored by CV in an acetonitrile solution of ferrocene (1 mM) and tetrabutylammonium hexafluorophosphate (0.1 M) with a scan rate of 100 mV s^{-1} between +0.10 and +0.70 V (vs Ag/AgCl). CVs of a ferrocene redox reaction were found to be almost identical for bare- and alkyne-terminated BDD (Figure 2B; red and green, respectively). On the other hand, for TIPS-terminated BDD, the peak-to-peak potential separation became larger accompanied by a decrease in both oxidation and reduction peak currents (Figure 2B; blue), which indicates that bulky TIPS groups inhibit electron transfer between BDD and ferrocene in solution. As a whole, it is suggested that the immobilized organic layer is thin and presents a low barrier for electron transfer, consistent with previous reports for organic-molecule-modified glassy carbon electrodes.[51,56] In addition, XPS showed that the Si(2p) peak from the TIPS group disappeared after deprotection (Figure 2C; green), also indicating formation of alkyne-terminated BDD.

As the third step, azobenzene (AZ) was immobilized by a click reaction, copper(I)-catalyzed Huisgen 1,3-dipolar cycloaddition of azide and alkyne.[52] The click reaction was performed by immersing alkyne-terminated BDD for 24 h at room temperature into a dimethylformamide solution containing azide-terminated AZ (50 mM), copper(II) sulfate pentahydrate (5 mM), and L(+)-ascorbic acid (7.5 mM) as a reducing agent of copper(II). After the click reaction, CV of AZ-terminated BDD was recorded in 1:1 isopropylalcohol/water containing acetic acid (0.5 M) and sodium acetate (0.5 M) with a scan rate of 50 mV s^{-1} between +0.40 and +1.00 V (vs Ag/AgCl). A clear oxidation peak was observed at +0.70 V (Figure 3A), ascribed to a two-step oxidation, involving two electrons in total, of a phenolic hydroxyl group in AZ to a phenoxy radical and then a phenoxy cation.[57] In addition, the XPS spectrum (Figure 3B) showed a strong N(1s) peak for AZ-terminated BDD, indicating immobilization of AZ onto BDD. Here, surface concentration of AZ (Γ_{AZ}) can be calculated by the equation $\Gamma_{AZ} = Q/(n\ F\ A)$, where Q is a passed charge derived from integration of the oxidation current, n is the number of electrons involved in the reaction, F is the Faraday constant, and A is a geometric surface area of the AZ-terminated BDD electrode. As a result, the Γ_{AZ} value was estimated to be 7.75×10^{-11} mol cm^{-2}. Assuming a two-dimensional packing of a rod-shaped *trans*-AZ with a diameter of 11.5 Å on a flat diamond surface, the maximum surface concentration can be given by 1.16×10^{-10} mol cm^{-2}, which is close to the obtained surface concentration. Therefore, it is suggested that AZ forms a densely packed monolayer onto BDD.

Recently, photoisomerization of azobenzene has been monitored by an electrochemical measurement.[58] Briefly, steric hindrance introduced by surface modification should reduce

dx.doi.org/10.1021/am5074613 | ACS Appl. Mater. Interfaces 2015, 7, 887−894

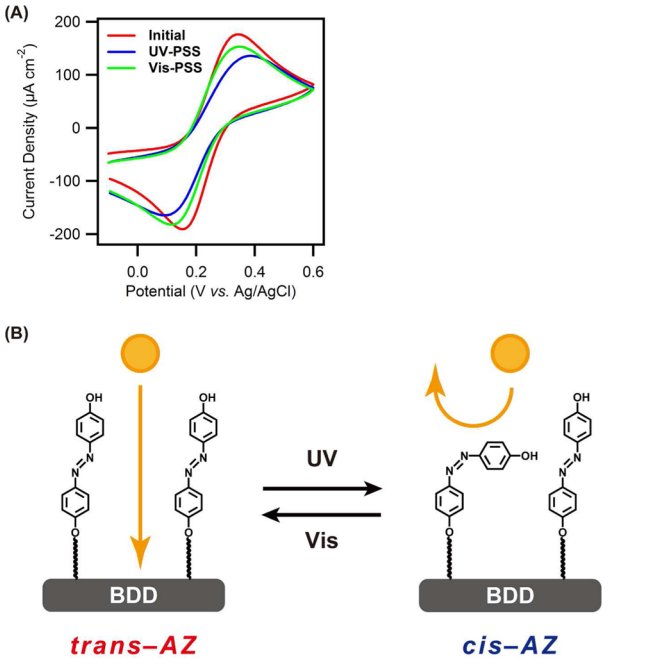

(C)

	Initial State	Photostationary State after UV Irradiation	Photostationary State after Vis Irradiation
I_a (μA cm^{-2})	176	136	153
E_a (mV)	0.345	0.385	0.350
I_c (μA cm^{-2})	−191	−165	−182
E_c (mV)	0.155	0.090	0.115
ΔE_p (mV)	0.190	0.295	0.235

Figure 4. Photoisomerization of AZ immobilized onto the BDD surface. (A) CVs in an aqueous solution of potassium ferricyanide ($K_3[Fe^{III}(CN)_6]$): the initial state (red), the photostationary state after UV light irradiation (blue), and the photostationary state after visible light irradiation (green). Blocking was enhanced upon UV light irradiation (*trans*-to-*cis* isomerization; blue), and reversed upon visible light irradiation (*cis*-to-*trans* isomerization; green). (B) A schematic illustration of a blocking property in the AZ-terminated BDD electrode upon photoisomerization, where the probe molecule ($K_4[Fe^{II}(CN)_6]/K_3[Fe^{III}(CN)_6]$ redox couples) is denoted as an orange sphere. (C) A summarized table of electrochemical behaviors for the AZ-terminated BDD electrode; I_a and E_a denote anodic peak current density and potential, respectively, I_c and E_c denote cathodic peak current density and potential, respectively, and ΔE_p denotes the peak-to-peak potential separation.

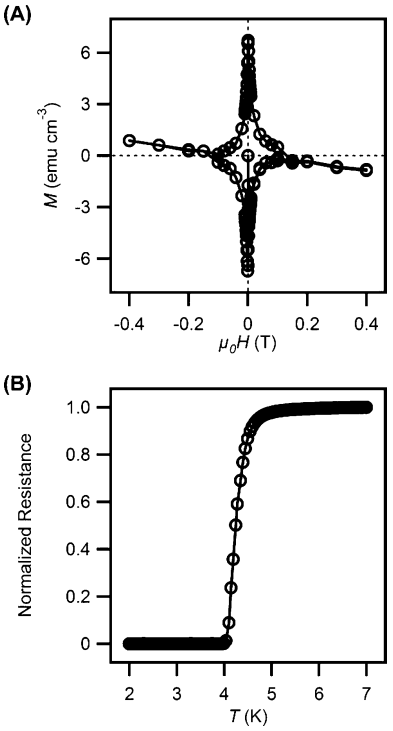

Figure 5. Superconducting properties of AZ-terminated BDD. (A) The field-dependent magnetization measured at 2.0 K to ±0.4 T. (B) The temperature-dependent resistance measured under zero magnetic field, where resistance was normalized using the value at 7.0 K. The superconducting properties of BDD were preserved after immobilization of AZ.

pinholes in the electrode, enhancing the blocking character. As photoisomerization of azobenzene accompanies volume changes in the molecular structure, pinholes would become smaller for the bent-shaped, larger *cis*-isomer. In such a case, it is possible to deduce the photoisomerization process by electrochemical measurements using a redox couple, ferrocyanide ($[Fe^{II}(CN)_6]^{4-}$) ions/ferricyanide ions ($[Fe^{III}(CN)_6]^{3-}$), which is known to be highly sensitive to surface modification due to the inner-sphere electron-transfer character.[56] Along these lines, we monitored photoisomerization of AZ immobilized onto BDD by CV measurements in an aqueous solution of potassium ferricyanide ($K_3[Fe^{III}(CN)_6]$; 1 mM) and potassium chloride (0.1 M) with a scan rate 100 mV s^{-1} between −0.10 and +0.60 V versus Ag/AgCl. Figure 4A shows CVs for the initial state, upon UV light irradiation, and upon visible light irradiation. Upon UV light irradiation, there is a decrease of peak current density and an increase in the peak-to-peak potential separation (ΔE_p), indicating blocking enhancement of the AZ-terminated BDD electrode, which is ascribed to photoisomerization to the bent-shaped, larger *cis*-isomer, decreasing pinhole area at the AZ-terminated BDD surface (Figure 4B; Right). On the other hand, upon visible light irradiation, there is a recovery of peak current density and ΔE_p, indicating the enhanced blocking property is reversed by subsequent photoisomerization back to the rod-shaped, smaller *trans*-isomer. So, there is reversible modulation of blocking properties upon alternate UV and visible light irradiation. Figure 4C summarizes values of peak current densities, peak potentials, and ΔE_p for each photostationary state. Note that the above results are nearly consistent with the previous report for an azobenzene-immobilized glassy carbon electrode.[58]

Superconducting properties of AZ-terminated BDD were investigated with magnetic and electrical transport measurements. Figure 5A shows the field-dependent magnetization measured at 2.0 K to ±0.4 T, where a magnetic hysteresis loop was observed with a nearly symmetric rhomboid shape, which is characteristic of a type-II superconductor. In addition, Figure 5B shows the temperature dependence of resistance measured under zero magnetic field, where resistance was normalized using the value at 7.0 K. Resistance decreased gradually from ∼4.6 K, corresponding to an onset of a superconducting transition (T_C-onset), and zero resistance was achieved at 4.0 K (T_C-offset). Therefore, the superconducting properties of BDD were preserved after immobilization of AZ. Subsequently, we examined the effect of AZ photoisomerization by measuring temperature dependence of resistance under zero magnetic field after UV light irradiation, and after a subsequent

dx.doi.org/10.1021/am5074613 | ACS Appl. Mater. Interfaces 2015, 7, 887−894

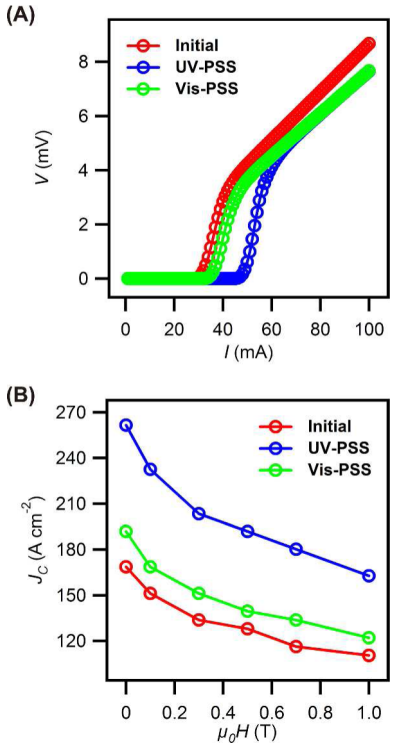

Figure 6. (A) Voltage−current responses (V−I curves) of AZ-terminated BDD at 2.0 K under zero magnetic field: the initial state (red), the photostationary state after UV light irradiation (blue), and the photostationary state after visible light irradiation (green). The critical current is determined at which a voltage starts to arise with a 10 μV criterion from V−I curves. (B) The critical current density (J_C) was plotted as a function of a magnetic field from 0 to 1.0 T. The J_C of AZ-terminated BDD were amplified by 55% after UV light irradiation (blue) and recovered after visible light irradiation (green).

visible light irradiation, to reveal that both T_C-onset and T_C-offset were unchanged. We posit that the massive nature of the 4 μm BDD film renders the T_C impervious to photoisomerization-induced changes in surface electronic states. To probe a different aspect of the superconducting state, a voltage−current response that is sensitive to the critical current density was measured at 2.0 K under various magnetic fields by applying a current from 1 mA to 100 mA with 1 mA increments (a V−I curve). Figure 6A shows V−I curves for the initial state (Figure 6A, red), after UV light irradiation (Figure 6A, blue), and also after a subsequent visible light irradiation (Figure 6A, green) at 2.0 K under zero magnetic field. Here, a critical current is defined at which a voltage starts to arise with a 10 μV criterion from a V−I curve. Critical current density (J_C) was calculated by dividing the critical current by the cross-sectional area (0.43 cm × 4 μm) of AZ-terminated BDD. Figure 6B shows the J_C as a function of a magnetic field from 0 to 1.0 T, where the J_C increased after UV light irradiation, and recovered after visible light irradiation. This striking change corresponds to reversible amplification of the J_C by 55% upon photoisomerization.

Here, we discuss why the J_C could be modulated upon photoisomerization of immobilized AZ. In type-II superconducting films, the surface-pinning potential is so strong that the surface-pinning force is comparable to that in a bulk superconductor because of nonuniformity of electron density along the surface.[59] This dominance of surface pinning is most pronounced in the superconducting state just below T_C where bulk pinning is weakest. In our experiments, the T_C value of AZ-terminated BDD was found to be 4.0 K, and the J_C value determined by V−I curves was measured at 2.0 K. In this temperature regime, modulation of the J_C could be due to surface pinning, even for relatively thick 4 μm superconducting BDD. On the other hand, a T_C would be robust with respect to such a surface effect as a T_C is a bulk property. In general, when an organic monolayer is formed on a type-II superconducting film, charge transfer occurs from the superconductor to the organic layers, resulting in a uniform distribution of charge density along the surface.[38] Therefore, changes in electron density at the film surface due to charge transfer could lead to modulation of the J_C. The proposed reversible charge transfer between BDD and immobilized AZ in this report is further justified by our previous report that showed the work function of gold can be modulated upon photoisomerization of azobenzene, where *trans*- and *cis*-isomers of the azobenzene monolayer on the gold substrate have different dipole moments.[24]

So, upon UV light irradiation (*trans*-to-*cis* isomerization), charge transfer occurs from the AZ molecular layer to BDD due to a positive surface dipole moment of the *cis*-isomer of AZ. Such a charge-transfer process induces an inhomogeneous electron distribution at the BDD surface because both *trans*- and *cis*-isomers of AZ are present after UV light irradiation due to the incomplete solid-state *trans*-to-*cis* isomerization.[60] It is this inhomogeneous electron distribution along the BDD surface that can lead to significant photoamplification of the J_C. After visible light irradiation, the J_C recovers as homogeneity returns to the BDD surface with a reverse photoisomerization back to the original state. This mechanism is supported by our previous report, in which the J_C of hydrogen-terminated BDD were larger than that of oxygen-terminated BDD.[50] Briefly, hydrogen-terminated BDD has higher surface hole density than oxygen-terminated BDD due to formation of a hole accumulation layer at the surface.[49] In other words, the higher J_C of hydrogen-terminated BDD is ascribed to an inhomogeneous electron distribution induced by a hole accumulation layer.

The BDD and AZ composite has significant differences from the previous niobium and azobenzene composite[42] that we highlight here. First, the J_C of BDD was amplified by 55% upon *trans*-to-*cis* isomerization, which is more than 4 times higher than the previous report on niobium (13%). Second, the thickness of the superconducting material is quite different (ca. 4 μm for BDD, and 10 nm for niobium). Therefore, photoamplification of the J_C in BDD may be enhanced by reducing the thickness to the nanometer regime. Third, surface concentration of immobilized azobenzene was clearly demonstrated, while not estimated in the previous report. As a result, the inhomogeneous electron distribution induced upon photoisomerization could be analyzed quantitatively by changing surface concentration of azobenzene.

CONCLUSION

In summary, we have prepared a photoswitchable superconductor composite made from a heavily boron-doped diamond (BDD) and a photochromic azobenzene (AZ) molecular layer by an electrochemical immobilization method and a click reaction. We have observed a reversible change in critical current density (J_C) with UV−visible light irradiation. This change is most likely due to photoisomerization of AZ inducing an inhomogeneous electron distribution along the BDD surface. Even for relatively thick superconducting BDD (thickness: ca.

dx.doi.org/10.1021/am5074613 | ACS Appl. Mater. Interfaces 2015, 7, 887−894

4 μm), the J_C was amplified by 55% upon *trans*-to-*cis* isomerization, which was found to be more than 4 times higher than that of our previous report on a much thinner sample[42] (i.e., 13% for the 10 nm thick niobium−azobenzene photoswithcable superconductor). Such a significant photoamplification in the J_C might be unique for BDD because of "surface-sensitive" superconducting properties of BDD.[50] This surface sensitivity highlights the novel tunability of BDD that may be enhanced in thinner films. As a next step, it might be possible to observe much more drastic modulation by fabricating a lamellar heterostrucure of BDD with photo- and/or electroactive materials.

AUTHOR INFORMATION

Corresponding Authors

*E-mail: takyama@chem.keio.ac.jp. (T.Y.)

*E-mail: einaga@chem.keio.ac.jp. (Y.E.)

Author Contributions

K.N. prepared boron-doped diamonds, synthesized organic compounds, and examined superconducting properties. M.A. prepared surface-modified boron-doped diamonds and carried out electrochemical measurements. T.Y. and Y.E. directed the research, discussing results and analyses. K.N. and T.Y. wrote the manuscript through contributions of all authors. All authors have read and given approval to the final version of the manuscript.

Notes

The authors declare no competing financial interest.

ACKNOWLEDGMENTS

This work was supported by Grant-in-Aid for Scientific Research on Innovative Areas ("Coordination Programming" Area 2107, Grant No. 24108736) from MEXT of Japan and for Young Scientist (B, Grant No. 25810142) from JSPS of Japan. We thank D. M. Pajerowski for critical review of this manuscript during his stay in our group as a JSPS Short-term Fellow.

REFERENCES

(1) Browne, W. R.; Feringa, B. L. Light Switching of Molecules on Surfaces. *Annu. Rev. Phys. Chem.* **2009**, *60*, 407−428.

(2) Sun, S.-S.; Lees, A. J. Transition Metal Based Supramolecular Systems: Synthesis, Photophysics, Photochemistry and Their Potential Applications as Luminescent Anion Chemosensors. *Coord. Chem. Rev.* **2002**, *230*, 171−192.

(3) Sauvage, J.-P. Transition Metal-Containing Rotaxanes and Catenanes in Motion: Toward Molecular Machines and Motors. *Acc. Chem. Res.* **1998**, *31*, 611−619.

(4) Dong, H.; Zhu, H.; Meng, Q.; Gong, X.; Hu, W. Organic Photoresponse Materials and Devices. *Chem. Soc. Rev.* **2012**, *41*, 1754−1808.

(5) Sato, O.; Hayami, S.; Einaga, Y.; Gu, Z.-Z. Control of the Magnetic and Optical Properties in Molecular Compounds by Electrochemical, Photochemical and Chemical Methods. *Bull. Chem. Soc. Jpn.* **2003**, *76*, 443−470.

(6) Gütlich, P.; Garcia, Y.; Woike, T. Photoswitchable Coordination Compounds. *Coord. Chem. Rev.* **2001**, *219−221*, 839−879.

(7) Beharry, A. A.; Woolley, G. A. Azobenzene Photoswitches for Biomolecules. *Chem. Soc. Rev.* **2011**, *40*, 4422−4437.

(8) Mayer, G.; Heckel, A. Biologically Active Molecules with a "Light Switch. *Angew. Chem., Int. Ed.* **2006**, *45*, 4900−4921.

(9) Willner, I. Photoswitchable Biomaterials: En Route to Optobioelectronic Systems. *Acc. Chem. Res.* **1997**, *30*, 347−356.

(10) *Molecular Switches;* Feringa, B. L., Ed.; Wiley-VCH: Weinheim, Germany, 2001.

(11) Irie, M. Diarylethenes for Memories and Switches. *Chem. Rev.* **2000**, *100*, 1685−1716.

(12) Matsuda, K.; Irie, M. Diarylethene as a Photoswitching Unit. *J. Photochem. Photobiol. C* **2004**, *5*, 169−182.

(13) Tian, H.; Yang, S. Recent Progresses on Diarylethenes Based Photochromic Switches. *Chem. Soc. Rev.* **2004**, *33*, 85−97.

(14) Irie, M. Photochromism: Memories and Switches. *Chem. Rev.* **2000**, *100*, 1683−1684.

(15) Matsuda, K.; Yamaguchi, H.; Sakano, T.; Ikeda, M.; Tanifuji, N.; Irie, M. Conductance Photoswitching of Diarylethene-Gold Nanoparticle Network Induced by Photochromic Reaction. *J. Phys. Chem. C* **2008**, *112*, 17005−17010.

(16) Ikeda, M.; Tanifuji, N.; Yamaguchi, H.; Irie, M.; Matsuda, K. Photoswitching of Conductance of Diarylethene-Au Nanoparticle Network. *Chem. Commun.* **2007**, 1355−1357.

(17) Boyer, J.-C.; Carling, C.-J.; Gates, B. D.; Branda, N. R. Two-Way Photoswitching Using One Type of Near-Infrared Light, Upconverting Nanoparticles, and Changing Only the Light Intensity. *J. Am. Chem. Soc.* **2010**, *132*, 15766−15772.

(18) Carling, C.-J.; Boyer, J.-C.; Branda, N. R. Remote-Control Photoswitching Using NIR Light. *J. Am. Chem. Soc.* **2009**, *131*, 10838−10839.

(19) Crivillers, N.; Orgiu, E.; Reinders, F.; Mayor, M.; Samori, P. Optical Modulation of the Charge Injection in an Organic Field-Effect Transistor Based on Photochromic Self-Assembled-Monolayer-Functionalized Electrodes. *Adv. Mater.* **2011**, *23*, 1447−1452.

(20) Shen, Q.; Cao, Y.; Liu, S.; Steigerwald, M. L.; Guo, X. Conformation-Induced Electrostatic Gating of the Conduction of Spiropyran-Coated Organic Thin-Film Transistors. *J. Phys. Chem. C* **2009**, *113*, 10807−10812.

(21) Suda, M.; Kameyama, N.; Suzuki, M.; Kawamura, N.; Einaga, Y. Reversible Phototuning of Ferromagnetism at Au−S Interfaces at Room Temperature. *Angew. Chem., Int. Ed.* **2008**, *47*, 160−163.

(22) Suda, M.; Nakagawa, M.; Iyoda, T.; Einaga, Y. Reversible Photoswitching of Ferromagnetic FePt Nanoparticles at Room Temperature. *J. Am. Chem. Soc.* **2007**, *129*, 5538−5543.

(23) Yamamoto, T.; Umemura, Y.; Einaga, Y. Structure-Distortion-Induced Photomagnetic Effect in Azobenzene/Polyoxometalate Langmuir−Blodgett Films. *Dalton Trans.* **2013**, *42*, 16014−16020.

(24) Suda, M.; Kameyama, N.; Ikegami, A.; Einaga, Y. Reversible Phototuning of the Large Anisotropic Magnetization at the Interface between a Self-Assembled Photochromic Monolayer and Gold. *J. Am. Chem. Soc.* **2009**, *131*, 865−870.

(25) Suda, M.; Einaga, Y. Sequential Assembly of Phototunable Ferromagnetic Ultrathin Films with Perpendicular Magnetic Anisotropy. *Angew. Chem., Int. Ed.* **2009**, *48*, 1754−1757.

(26) Yamamoto, T.; Umemura, Y.; Sato, O.; Einaga, Y. Photoswitchable Magnetic Films: Prussian Blue Intercalated in Langmuir−Blodgett Films Consisting of an Amphiphilic Azobenzene and a Clay Mineral. *Chem. Mater.* **2004**, *16*, 1195−1201.

(27) Onnes, K. H. Further Experiments with Liquid Helium. G. On the Electrical Resistance of Pure Metals, etc. VI. On the Sudden Change in the Rate at which the Resistance of Mercury Disappears. *Commun. Phys. Lab. Univ. Leiden* **1911**, 124c; reprinted in: *Proc. K. Akad. Wet.* **1912**, *14*, 818−821.

(28) Timusk, T.; Statt, B. The Pseudogap in High-Temperature Superconductors: an Experimental Survey. *Rep. Prog. Phys.* **1999**, *62*, 61−122.

(29) Dagotto, E. Correlated Electrons in High-Temperature Superconductors. *Rev. Mod. Phys.* **1994**, *66*, 763−840.

(30) Larbalestier, D.; Gurevich, A.; Feldmann, D. M.; Polyanskii, A. High-T_C Superconducting Materials for Electric Power Applications. *Nature* **2001**, *414*, 368−377.

(31) Clarke, J.; Wilhelm, F. K. Superconducting Quantum Bits. *Nature* **2008**, *453*, 1031−1042.

(32) Kamihara, Y.; Watanabe, T.; Hirano, M.; Hosono, H. Iron-Based Layered Superconductor La$[O_{1-x}F_x]$FeAs (x = 0.05−0.12) with T_C = 26 K. *J. Am. Chem. Soc.* **2008**, *130*, 3296−3297.

(33) Monteverde, M.; Acha, C.; Núñez-Regueiro, M.; Pavlov, D. A.; Lokshin, K. A.; Putilin, S. N.; Antipov, E. V. High-Pressure Effects in Fluorinated $HgBa_2Ca_2Cu_3O_{8+\delta}$. *Europhys. Lett.* **2005**, *72*, 458−464.

(34) Bardeen, J.; Cooper, L. N.; Schrieffer, J. R. Theory of Superconductivity. *Phys. Rev.* **1957**, *108*, 1175−1204.
(35) Ueno, K.; Nakamura, S.; Shimotani, H.; Ohtomo, A.; Kimura, N.; Nojima, T.; Aoki, H.; Iwasa, Y.; Kawasaki, M. Electric-Field-Induced Superconductivity in an Insulator. *Nat. Mater.* **2008**, *7*, 855−858.
(36) Takahashi, K. S.; Gabay, M.; Jaccard, D.; Shibuya, K.; Ohnishi, T.; Lippmaa, M.; Triscone, J.-M. Local Switching of Two-Dimensional Superconductivity Using the Ferroelectric Field Effect. *Nature* **2006**, *441*, 195−198.
(37) Ahn, C. H.; Triscone, J.-M.; Mannhart, J. Electric Field Effect in Correlated Oxide Systems. *Nature* **2003**, *424*, 1015−1018.
(38) Cahen, D.; Naaman, R.; Vager, Z. The Cooperative Molecular Field Effect. *Adv. Funct. Mater.* **2005**, *15*, 1571−1578.
(39) Zhang, Y.; Terrill, R. H.; Bohn, P. W. Chemisorption and Chemical Reaction Effects on the Resistivity of Ultrathin Gold Films at the Liquid-Solid Interface. *Anal. Chem.* **1999**, *71*, 119−125.
(40) Cohen, R.; Kronik, L.; Shanzer, A.; Cahen, D.; Liu, A.; Rosenwaks, Y.; Lorenz, J. K.; Ellis, A. B. Molecular Control over Semiconductor Surface Electronic Properties: Dicarboxylic Acids on CdTe, CdSe, GaAs, and InP. *J. Am. Chem. Soc.* **1999**, *121*, 10545−10553.
(41) Shvarts, Dm.; Hazani, M.; Shapiro, B. Ya.; Leitus, G.; Sidorov, V.; Naaman, R. Molecular Induced Field Effect in Superconducting Nb Films. *Europhys. Lett.* **2005**, *72*, 465−471.
(42) Ikegami, A.; Suda, M.; Watanabe, T.; Einaga, Y. Reversible Optical Manipulation of Superconductivity. *Angew. Chem., Int. Ed.* **2010**, *49*, 372−374.
(43) Bullock, D. J. W.; Cumper, C. W. N.; Vogel, A. I. Physical Properties and Chemical Constitution. Part XLIII. The Electric Dipole Moments of Azobenzene, Azopyridines, and Azoquinolines. *J. Chem. Soc.* **1965**, 5316−5323.
(44) Carmeli, I.; Lewin, A.; Flekser, E.; Diamant, I.; Zhang, Q.; Shen, J.; Gozin, M.; Richter, S.; Dagan, Y. Tuning the Critical Temperature of Cuprate Superconductor Films with Self-Assembled Organic Layers. *Angew. Chem., Int. Ed.* **2012**, *51*, 7162−7165.
(45) Ekimov, E. A.; Sidorov, V. A.; Bauer, E. D.; Mel'nik, N. N.; Curro, N. J.; Thompson, J. D.; Stishov, S. M. Superconductivity in Diamond. *Nature* **2004**, *428*, 542−545.
(46) McMillan, W. L. Transition Temperature of Strong-Coupled Superconductors. *Phys. Rev.* **1968**, *167*, 331−344.
(47) Takano, Y. Superconductivity in CVD Diamond Films. *J. Phys.: Condens. Matter.* **2009**, *21*, 253201−11pp.
(48) Szunerits, S.; Boukherroub, R. Different Strategies for Functionalization of Diamond Surfaces. *J. Solid State Electrochem.* **2008**, *12*, 1205−1218.
(49) Maier, F.; Riedel, M.; Mantel, B.; Ristein, J.; Ley, L. Origin of Surface Conductivity in Diamond. *Phys. Rev. Lett.* **2000**, *85*, 3472−3475.
(50) Natsui, K.; Yamamoto, T.; Watanabe, T.; Kamihara, Y.; Einaga, Y. Modulation of Critical Current Density in Polycrystalline Boron-Doped Diamond by Surface Modification. *Phys. Status Solidi B* **2013**, *250*, 1943−1949.
(51) Leroux, Y. R.; Fei, H.; Noël, J.-M.; Roux, C.; Hapiot, P. Efficient Covalent Modification of a Carbon Surface: Use of a Silyl Protecting Group To Form an Active Monolayer. *J. Am. Chem. Soc.* **2010**, *132*, 14039−14041.
(52) Kolb, H. C.; Finn, M. G.; Sharpless, K. B. Click Chemistry: Diverse Chemical Function from a Few Good Reactions. *Angew. Chem., Int. Ed.* **2001**, *40*, 2004−2021.
(53) Anderson, S. Phenylene Ethynylene Pentamers for Organic Electroluminescence. *Chem.—Eur. J.* **2001**, *7*, 4706−4714.
(54) Wei, W.-H.; Tomohiro, T.; Kodaka, M.; Okuno, H. Selective Synthesis and Kinetic Measurement of 1:1 and 2:2 Cyclic Compounds Containing 1,4,7,10-Tetraazacyclododecane and Azobenzene Units. *J. Org. Chem.* **2000**, *65*, 8979−8987.
(55) Niu, L.; Zhu, J.-Q.; Han, X.; Tan, M.-L.; Gao, W.; Du, S.-Y. First Principles Study of Structural, Electronic and Vibrational Properties of Heavily Boron-Doped Diamond. *Phys. Lett. A* **2009**, *373*, 2494−2500.
(56) Chen, P.; McCreery, R. L. Control of Electron Transfer Kinetics at Glassy Carbon Electrodes by Specific Surface Modification. *Anal. Chem.* **1996**, *68*, 3958−3965.
(57) Rodrigo, M. A.; Michaud, P. A.; Duo, I.; Panizza, M.; Cerisola, G.; Comninellis, Ch. Oxidation of 4-Chlorophenol at Boron-Doped Diamond Electrode for Wastewater Treatment. *J. Electrochem. Soc.* **2001**, *148*, D60−D64.
(58) Leroux, Y. R.; Hapiot, P. Photo-Modulation of the Permeation in Azobenzene Derivatives Monolayer Films Electrografted on Carbon Substrates. *Electrochem. Commun.* **2013**, *33*, 107−110.
(59) Mishra, P. K.; Ravikumar, G.; Sahni, V. C.; Koblischka, M. R.; Grover, A. K. Surface Pinning in Niobium and a High-T_C Superconductor. *Phys. C* **1996**, *269*, 71−75.
(60) Naito, T.; Horie, K.; Mita, I. Photochemistry in Polymer Solids. 11. The Effects of the Size of Reaction Groups and the Mode of Photoisomerization on Photochromic Reactions in Polycarbonate Film. *Macromolecules* **1991**, *24*, 2907−2911.